IEEE Photonics Journal
An IEEE Photonics Society Publication

Open Access

Single Channel 50 Gbit/s Transmission Over 40 km SSMF Without Optical Amplification and In-Line Dispersion Compensation Using a Single-End PD-Based PDM-SSB-DMT System

Volume 9, Number 5, October 2017

Xian Zhou
Jiahao Huo
Kangping Zhong
Faisal Nadeem Khan
Tao Gui
Hongyu Zhang
Jiajing Tu
Jinhui Yuan
Keping Long
Changyuan Yu
Alan Pak Tao Lau
Chao Lu

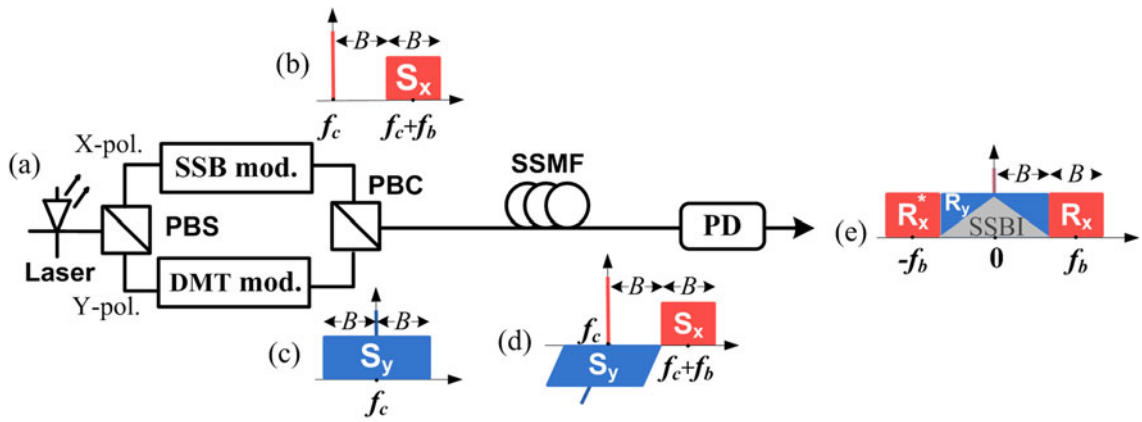

DOI: 10.1109/JPHOT.2017.2749501
1943-0655 © 2017 IEEE

Single Channel 50 Gbit/s Transmission Over 40 km SSMF Without Optical Amplification and In-Line Dispersion Compensation Using a Single-End PD-Based PDM-SSB-DMT System

Xian Zhou,[1,2] Jiahao Huo,[1,2] Kangping Zhong,[1,2] Faisal Nadeem Khan,[3] Tao Gui,[3] Hongyu Zhang,[4] Jiajing Tu,[1,2] Jinhui Yuan,[2] Keping Long,[1] Changyuan Yu,[2] Alan Pak Tao Lau,[3] and Chao Lu[2]

[1]Beijing Engineering and Technology Center for Convergence Networks and Ubiquitous Services, University of Science & Technology Beijing, Beijing 100083, China
[2]Photonics Research Centre, Department of Electronic and Information Engineering, The Hong Kong Polytechnic University, Kowloon, Hong Kong, SAR
[3]Photonics Research Centre, Department of Electrical Engineering, The Hong Kong Polytechnic University, Kowloon, Hong Kong, SAR
[4]Fixed Network R&D Department, Huawei Technologies Co, Ltd., Shenzhen 518057, China

DOI:10.1109/JPHOT.2017.2749501

Manuscript received July 25, 2017; revised August 31, 2017; accepted September 2, 2017. Date of publication September 6, 2017; date of current version September 29, 2017. This work was supported in part by the National Natural Science Foundation of China under Grants 61671053, 61435006, and 61401020, in part by projects H-ZG46 and H-ZG3Y of PolyU and Huawei Technologies Co. Ltd., and in part by Fundamental Research Funds for the Central University FRF-TP-16-013A3. (X. Zhou and J. Huo contributed equally to this work.) Corresponding authors: X. Zhou and K. Zhong (e-mail: zhouxian219@gmail.com; zhongkangping1987@gmail.com).

Abstract: We experimentally demonstrate a single-end photodetector (PD) based polarization-division-multiplexing (PDM) system, in which the single-sideband orthogonal frequency-division multiplexing (SSB-OFDM) and discrete multitone (DMT) signals are modulated on two orthogonal polarizations respectively. Based on the frequency interleave design for dual-polarization, the spectral efficiency and chromatic dispersion tolerance can be optimized. We derive the theoretical model for the PDM-SSB-DMT system and detail the digital signal processing for demultiplexing at the receiver. We also successfully transmit a 50 Gb/s PDM-SSB-DMT signal with 14 GHz bandwidth over 40 km of uncompensated and unamplified standard single mode fiber (SSMF) with only 1.1 dB power penalty for a bit error rate of 3.8×10^{-3} relative to back-to-back transmissions.

Index Terms: Polarization-multiplexing, direct-detection, single-sideband, discrete multitone.

1. Introduction

With the increasing broadband mobile communications, cloud services, video applications and other high capacity storage and high speed applications, the transmission capacity demand is growing significantly for the data-center (DC) interconnects. Considering the cost, footprint

and power consumption requirements of DC interconnects, intensity-modulation direct-detection (IM-DD) is more attractive than coherent detection for short reach applications. In recent years, several high speed IM-DD transmission systems have been demonstrated employing advanced modulation formats including pulse amplitude modulation (PAM) [1]–[3], half-cycle quadrature amplitude modulation (QAM) [4], [5], carrier-less amplitude and phase modulation (CAP) [6], [7] and discrete multi-tone (DMT) [8], [9]. However, most of these systems are operated at the O-band (1310 nm) because there is negligible chromatic dispersion (CD) and acceptable loss for the short reach ($<$20 km). However, when the transmission distance approaches 40 km for extended reach (ER) inter-DC applications, it is difficult for O-band systems to meet the power budget requirement due to the severe fiber loss. Therefore, high speed long-reach direct-detection system is preferred to operate at C-band due to its lower loss. However, CD-induced frequency-selective power fading degrades system performance and severely restrict the achievable transmission rate. Among the previously mentioned IM-DD systems, DMT signals can use bit and power loading technique [10], [11] to customize modulation format for each subcarrier and maximize the spectral efficiency (SE). But, the power fading influence cannot be vanished, DMT systems still face the issue of reduction in available bandwidth and transmission capacity. Another option is CD pre-compensation at the transmitter employing IQ modulator [12], which can eliminate the influence of CD and allow high speed transmission over long distance for direct-detection systems. However, it is difficult to obtain the precise prior knowledge of the link's cumulative dispersion without using feedback mechanisms. Besides, the pre-distorted signals will increase the peak-to-average-power ratio (PAPR) [13] which is not desirable. An alternative option is single side band (SSB) modulation which is inherently immune to CD effects without the need of prior knowledge of the link's cumulative dispersion [14]. However, its photo-detection process will generate an unwanted component, i.e., the subcarrier-to-subcarrier beating interference (SSBI). In [15]–[17], a guard band between the carrier and SSB signal is used to avoid the nonlinear SSBI but results in the reduced spectral efficiency. Recently, several digital SSBI cancellation methods were proposed to remove the use of guard band, including pre-distortion [18], [19] or post-compensation [20], [21] approaches. However, their SSBI reconstruction processes have to use the received signal that are itself influenced by SSBI. In this case, the good performance of the SSBI cancellation will depend on high carrier-to-signal power ratio (CSPR) ($>$10 dB) or multi-stage cancellation operations.

In order to increase the spectral efficiency for inter-DC applications, we proposed a single-end photo-detector (PD) based polarization-division-multiplexing (PDM) scheme in [22], which employs two different modulation formats (i.e., SSB-OFDM and DMT) on two orthogonal polarizations respectively. Based on the frequency interleave design for two polarizations, the spectral efficiency and chromatic dispersion (CD) tolerance can be optimized. In this paper, the proposed PDM-DD system is studied and experimentally demonstrated in more detail. Section 2 derives the theoretical model of the PDM-SSB-DMT system and proposes a simple SSBI cancellation algorithm for signal de-multiplexing, which is operated with feedforward in one stage and without high CSPR requirement. Afterwards, the key parameters of the proposed PDM-SSB-DMT system are experimentally studied in Section 3. Based on the optimized system setup, a 50 Gb/s PDM-SSB-DMT transmission in 14 GHz bandwidth over 40 km standard single mode fiber (SSMF) at C-band is successfully demonstrated without optical amplification and in-line CD compensation. Finally, conclusions are given in Section 4.

2. The Operating Principle of PDM-SSB-DMT

At the transmitter side, a SSB-OFDM signal is modulated on X polarization (X-pol.) with a guard band equals to the signal bandwidth B to avoid SSBI-induced impairments. The transmitted optical SSB signal can be expressed as

$$g_{SSB}(t) = \left(C_x + s_x(t)e^{j2\pi f_b t}\right) \cdot e^{j2\pi f_c t + j\varphi} \tag{1}$$

where C_x is the direct current (DC) bias, f_c and φ are the frequency and phase of the transmitter laser respectively, $s_x(t)$ is the transmitted OFDM signal, and f_b is the electrical center frequency of

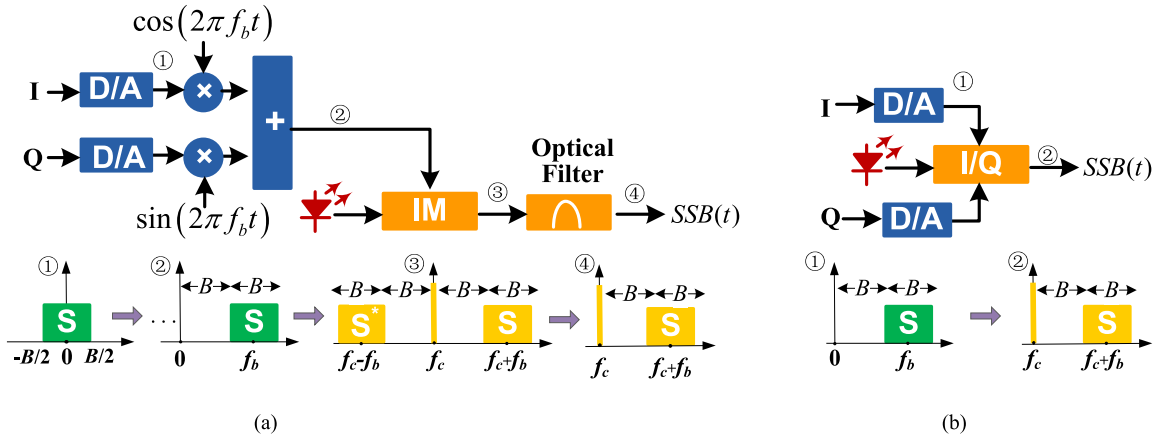

Fig. 1. Block diagrams of SSB signal transmitter by (a) using an electrical IQ mixer with intensity modulation and optical filter. (b) Using optical I/Q modulator.

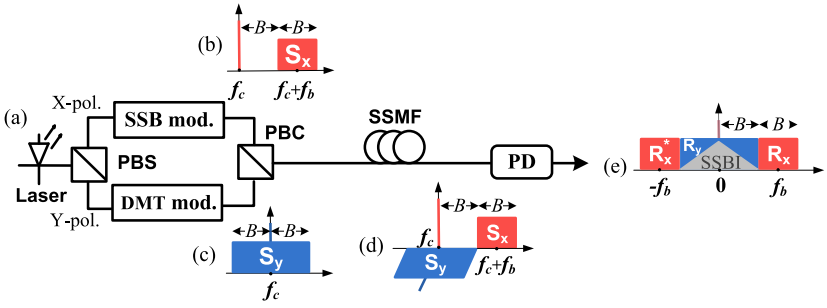

Fig. 2. (a) PDM-SSB-DMT-DD system architecture, and optical spectral diagrams of (b) SSB-OFDM, (c) DMT, (d) PDM-SSB-DMT signal, and (e) Electrical spectrum of the received PDM-SSB-DMT signal after direct detection. PBS: polarization beam splitter, PBC: polarization beam combiner.

$s_x(t)$ ($f_b = 1.5B$). The optical SSB signal can be generated either by using an intensity modulator (IM) with an optical filter [see Fig. 1(a)] or an optical I/Q modulator [see Fig. 1(b)]. We use the latter approach in our work.

Due to the presence of the guard band, the SSB modulation is achieved at the cost of reduced SE. In order to increase the SE, we put a DMT signal within the bandwidth of [$-B$, B] but in Y polarization (Y-pol) as shown in Fig. 2. The optical spectra of the SSB-OFDM and DMT signals are illustrated in Fig. 2(b) and (c), respectively. The DMT signal can be expressed as

$$g_{DMT}(t) = \sqrt{C_y + s_y(t)} \cdot e^{j2\pi f_c t + j\varphi} \tag{2}$$

where C_y is the DC bias in Y-pol and $s_y(t)$ is the baseband DMT signal. Then, the optical PDM-SSB-DMT signal is generated by combining the two signals using a polarization beam combiner (PBC).

At the receiver side, the PDM-SSB-DMT signal can be detected using a single-end PD. Since the SSB and DMT signals are in two orthogonal polarizations respectively, there is no inter-polarization beating interference product after a square-law detection. In this case, the detected current is given by

$$\begin{aligned} r(t) &= \left|(g_{SSB}(t) + g_{DMT}(t)) \otimes h(t)\right|^2 = \left|g_{SSB}(t) \otimes h(t)\right|^2 + \left|g_{DMT}(t) \otimes h(t)\right|^2 \\ &= \left|(C_x + s_x(t)e^{j2\pi f_b t}) \otimes h(t)\right|^2 + \left|\sqrt{C_y + s_y(t)} \otimes h(t)\right|^2 \end{aligned} \tag{3}$$

where $h(t)$ is the impulse response of the channel. The photodiode responsivity is assumed as 1 and noise is disregarded for simplicity purposes. In (3), the first term is the SSB-OFDM signal which

can be addressed as

$$\left|(C_x + s_x(t)e^{j2\pi f_b t}) \otimes h(t)\right|^2 = |C_x|^2 + C_x s_x(t)e^{j2\pi f_b t} \otimes h(t) + C_x s_x^*(t)e^{-j2\pi f_b t} \otimes h^*(t) + \left|s_x(t) \otimes h(t)\right|^2 \quad (4)$$

and the second term is the DMT signal, which can be expanded by Taylor's formula.

$$\left|\sqrt{C_y + s_y(t)} \otimes h(t)\right|^2 = \left|\left(\sqrt{C_y} + \frac{s_y(t)}{2\sqrt{C_y}} - \frac{s_y^2(t)}{8C_y^{3/2}} + \cdots\right) \otimes h(t)\right|^2 \quad (5)$$

Because high order terms can be suppressed by C_y and the DMT signal $s_y(t)$ is real valued, the (5) can be simplified as

$$\left|\sqrt{C_y + s_y(t)} \otimes h(t)\right|^2 \approx C_y + s_y(t) \otimes \frac{h(t) + h^*(t)}{2} \quad (6)$$

Next, denote $r_x(t) = s_x(t) \otimes h(t)$ and $r_y(t) = s_y(t) \otimes (\frac{h(t)+h^*(t)}{2})$. Then, after analog to digital conversion (ADC), the kth received sample can be addressed as

$$r(k) \approx \underbrace{\overbrace{|C_x|^2 + C_y}^{\text{dc}} + \overbrace{\left|r_x(k)\right|^2}^{SSBI} + \overbrace{r_y(k)}^{DMT}}_{Low\ Frequency} + \underbrace{\overbrace{C_x r_x(k)e^{j2\pi f_b k T_s} + C_x r_x^*(k)e^{-j2\pi f_b k T_s}}^{SSB-OFDM}}_{High\ Frequency} \quad (7)$$

where T_s is the sampling period. It can be seen from (7) that there are four products: 1) DC components that can be easily removed; 2) the SSB-induced 2nd-order nonlinear impairment - SSBI, 3) the detected DMT signal that overlaps with the SSBI in the same frequency band, and 4) the carrier-signal beating products which include the desired SSB-OFDM signal. The spectrum of the detected PDM-SSB-DMT signal is illustrated in Fig. 2(e). We have to extract $r_x(k)$ and $r_y(k)$ from $r(k)$ separately. Since they occupy different frequency bands, $r_x(k)$ can be extracted directly from the high frequency range $[B, 2B]$. However, the DMT signal $r_y(k)$ in baseband cannot be extracted in similar fashion as it is corrupted by SSBI. In this case, we introduce a feedforward SSBI cancellation algorithm to estimate and eliminate the SSBI and obtain the DMT signal.

Fig. 3 shows the detailed DSP configuration to de-multiplex the PDM-SSB-DMT signal. First, the received samples are converted into frequency domain. The DMT signal occupies the baseband frequency band from $-B$ to B while the high frequency band from B to $2B$ contains the SSB signal. Here, the down-sampling operations can also be implemented during the separation process. In addition, the frequency down conversion can be simultaneously performed for the SSB signal. Since the linear term of $r_x(k)$ is obtained in the first separation step and the SSBI scales quadratically with $r_x(k)$ as shown in (7), the SSBI impairment on the DMT signal can be easily reconstructed by the extracted SSB signal without any feedback iteration. However, due to the SSBI effects imposed on the frequencies of $[-B, B]$, the extracted SSB signal has to be expanded from $[-B/2, B/2]$ to $[-B, B]$ by padding zeros on its both sides in frequency domain to match the bandwidth of SSBI. This is equivalent to a two-fold up-sampling operation. This is followed by inverse fast Fourier transform (IFFT) and the corresponding SSB-OFDM and DMT signals in the time domain can be obtained as

$$r_{SSB}(k) = \overbrace{C_x r_x(k)}^{OFDM} \quad (8)$$

$$r_{DMT\_SSBI}(k) = \overbrace{|C_x|^2 + C_y}^{\text{dc}} + \overbrace{\left|r_x(k)\right|^2}^{SSBI} + \overbrace{r_y(k)}^{DMT} \quad (9)$$

Afterwards, the SSBI impairment can be reconstructed as

$$\hat{I}_{SSBI}(k) \approx \left|r_{SSB}(k)\right|^2 = |C_x|^2 \cdot \left|r_x(k)\right|^2 \quad (10)$$

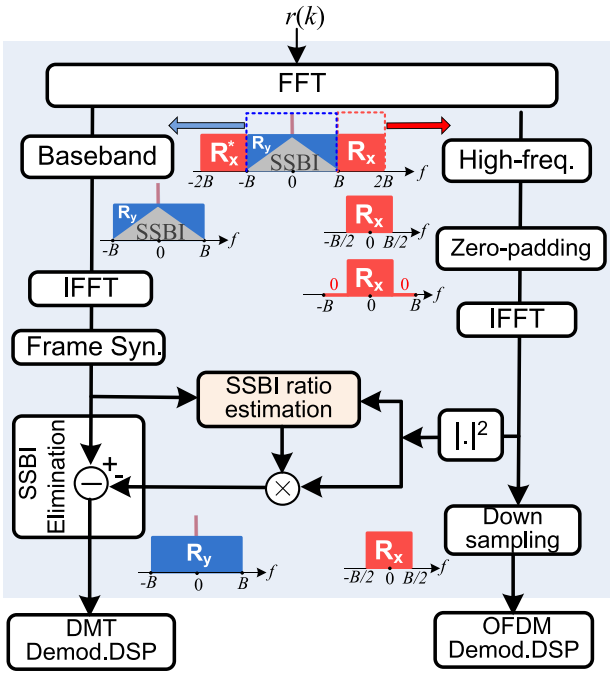

Fig. 3. The DSP configuration for signal de-multiplexing in the receiver.

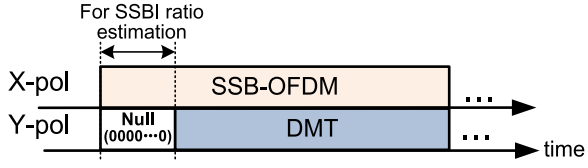

Fig. 4. The proposed frame structure of PDM-SSB-DMT signal.

However, due to the channel uncertainty in practice, the proportion between $|r_x(k)|^2$ and $\hat{I}_{SSBI}(k)$ will not be equal to $1/|C_x|^2$, which is unknown to the receiver. In this case, we introduce a ratio

$$|r_x(k)|^2 = A \cdot \hat{I}_{SSBI}(k) \tag{11}$$

where A denotes the proportion between the actual SSBI and the reconstructed SSBI. In order to estimate A, a PDM-SSB-DMT signal frame is designed as shown in Fig. 4. There are several zeros (null samples) inserted at the start of the DMT signal frame.

As shown in Fig. 4, after frame synchronization by calculating the correlation between the training and received DMT samples, the corresponding samples during the "null" period can be extracted and used to estimate the ratio as follow.

$$\hat{A} = \sum_{k=1}^{N} r'_{DMT\_SSBI}(k) \Big/ \sum_{k=1}^{N} |r_{SSB}(k)|^2 \tag{12}$$

where $\hat{A}$ is the estimated SSBI ratio, N is the number of zero samples, and r'_{DMT_SSBI} denotes r_{DMT_SSBI} after removing the DC term, which is given by

$$r'_{DMT\_SSBI}(k) = r_{DMT\_SSBI}(k) - \frac{1}{N} \sum_{k=1}^{N} r_{DMT\_SSBI}(k) \tag{13}$$

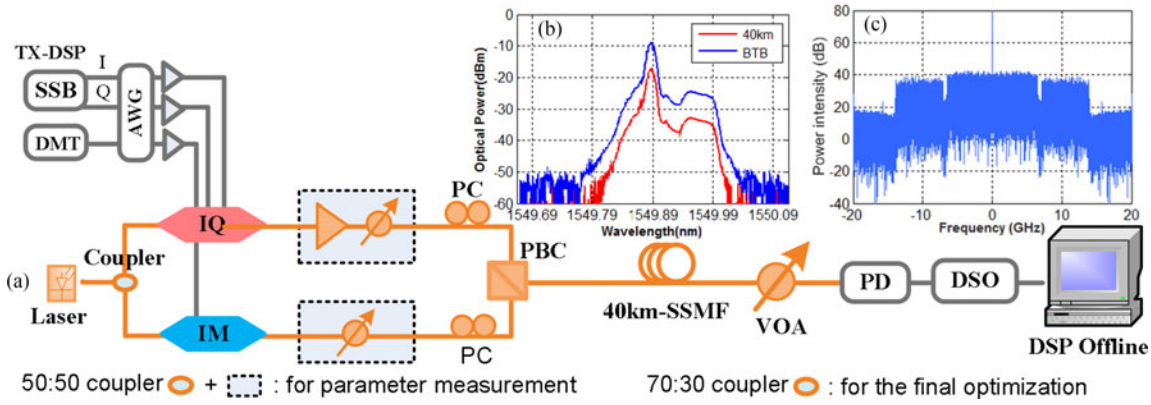

Fig. 5. (a) Experimental setup of the proposed PDM-SSB-DMT system. (b) The optical spectrum and (c) electrical spectrum of PDM-SSB-DMT signal.

Once the ratio A is estimated, the desired DMT signal can be obtained by subtracting the SSBI influence from r_{DMT_SSBI} as

$$r_{DMT}(k) = r_{DMT\_SSBI}(k) - \hat{A} \cdot \hat{I}_{SSBI}(k)_{,k=N+1,.....} \tag{14}$$

Subsequently, the DMT and the down-sampled SSB-OFDM signals can be separated and further processed accordingly to recover the information.

3. Experimental Setup and Results

Fig. 5(a) shows the experimental setup of the proposed PDM-SSB-DMT transmission system. At the transmitter, two pseudo-random binary sequences (PRBS) with length $2^{16} - 1$ are respectively mapped into uniform 16QAM for SSB-OFDM signal and adaptive M-QAM for DMT signal based on Fischer's bit-loading algorithm [11]. IFFT is used to obtain the time domain signals. Here, the IFFT size (i.e., the total number of subcarriers) is 128. For SSB-OFDM signal, 118 low-frequency subcarriers are loaded with the encoded data, and the remaining 10 subcarriers are filled zeros for oversampling to avoid aliasing. For DMT signal, the first subcarrier is the DC bias and the subcarriers 2 to 64 are loaded with data according to the adaptive bit-loading, and others are filled with the corresponding conjugate information to satisfy Hermitian symmetry. After conversion into time domain, six cyclic prefixes (CPs) are inserted to prevent inter-symbol interference (ISI) caused by channel dispersion. Subsequently, the real and imaginary parts of SSB-OFDM and DMT are up-sampled and uploaded into an arbitrary waveform generator (AWG) operated at 84 GSa/s for digital-to-analog (D/A) conversion. In our experiment, B is designed to be 7 GHz. Here, the electrical OFDM sideband signal occupies frequencies from 7 GHz to 14 GHz and the DMT signal with a bandwidth of 7 GHz occupies frequencies from 0 to 7 GHz.

A 15.5 dBm external cavity laser (ECL) at 1549.89 nm is split into two branches to modulate the SSB-OFDM and DMT using an IQ modulator and a dual-driver Mach-Zehnder modulator (DDMZM), respectively. During the period of parameter measurement, a 50:50 coupler is used here. In this case, the input power is 12.3 dBm for each modulator, and the output powers of the I/Q modulator and intensity modulator are -5.01 dBm and 2.32 dBm, respectively. Moreover, in order to adjust the output powers conveniently in this stage, an EDFA and a tunable attenuator are added in the SSB-OFDM branch, and another tunable attenuator is added in the DMT branch as shown in Fig. 5. When the optimum power assignment is found, a 70:30 coupler is used instead of the 50:50 coupler. Furthermore, the EDFA and tunable attenuators are also removed from the transmitter. For the SSB-OFDM branch, the IQ modulator is biased above the null point so as to maintain CSPR at 0 dB (CSPR [dB] $= 10\log_{10}$ (P_c/P_s), where P_c and P_s are the optical carrier and signal powers

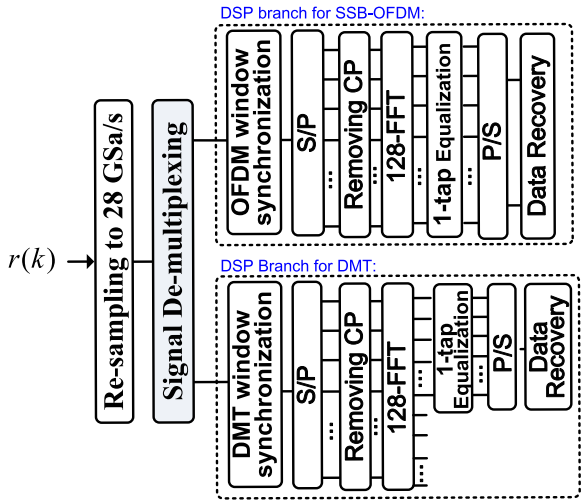

Fig. 6. DSP configuration for PDM-SSB-DMT signal.

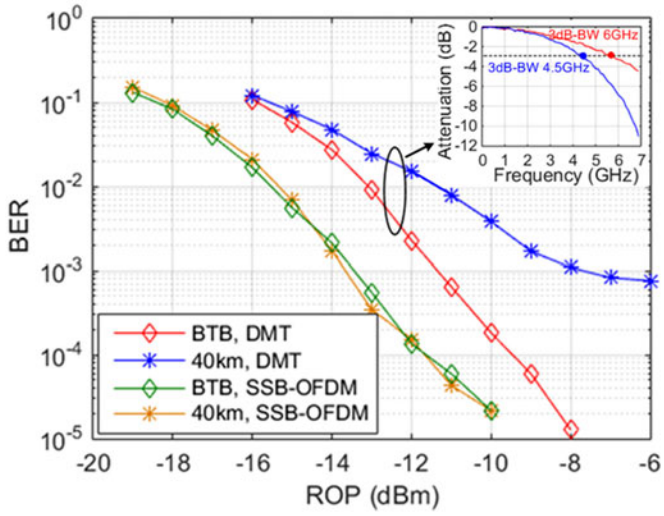

Fig. 7. BER performance as a function of ROP for the transmission with each single-polarization branch. Insert: the channel responses of DMT branch for the BTB and 40 km SSMF transmission.

respectively). Then, the two branches are combined with a PBC and launched into 0/40 km SSMF link. The overall PDM data rate is 50Gb/s, including 24.7 Gb/s (118 /(128 + 6)∗ 4 ∗ 7) SSB-OFDM and 25.3 Gb/s (63/(64 + 3) ∗ 3.85 ∗ 7) DMT. The optical spectrum of the PDM-SSB-DMT signal for BTB and after 40 km SSMF transmissions are illustrated in Fig. 5(b).

At the receiver side, a VOA is placed before the receiver to adjust the received optical power (ROP). Then, the optical signal is detected by a PIN+TIA receiver (3 dB bandwidth is 20 GHz) and sampled by a real-time scope at the sampling rate of 80 GSa/s with 33 GHz bandwidth and 8-bit resolution. The electrical spectrum of the received digital PDM-SSB-DMT signal is depicted Fig. 5(c). Subsequently, the offline DSP is implemented as shown in Fig. 6. Firstly, the digital PDM signal is re-sampled to 28 GSa/s (corresponding to 4*B*), and de-multiplexed to extract the SSB-OFDM and DMT signals (refer to Fig. 3). Then, the separated SSB-OFDM and DMT signals can be processed by their own demodulation DSP algorithms respectively, as shown in Fig. 6.

Fig. 7 shows the measured BER of each single polarization channel as a function of ROP for BTB and after 40 km transmissions. It can be seen that the DMT signal has an obvious BER

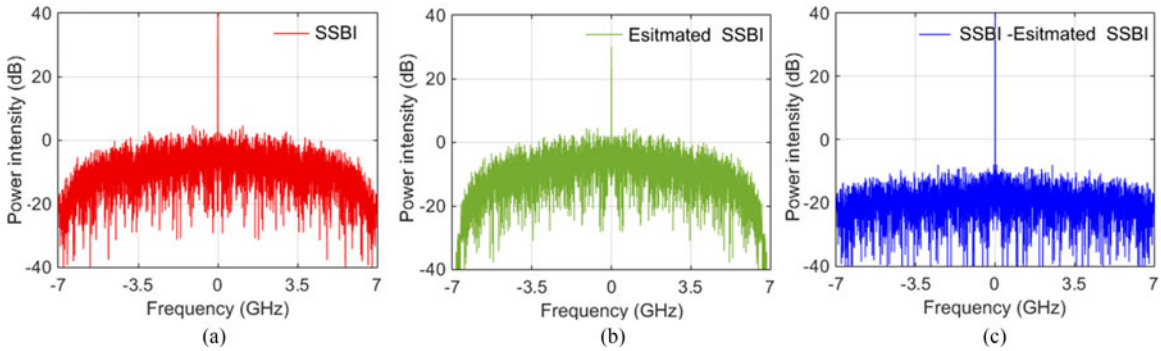

Fig. 8. Illustration of SSBI elimination ability, the electrical spectra of (a) the existed SSBI distortion (b) the estimated SSBI component (c) the signal after SSBI elimination.

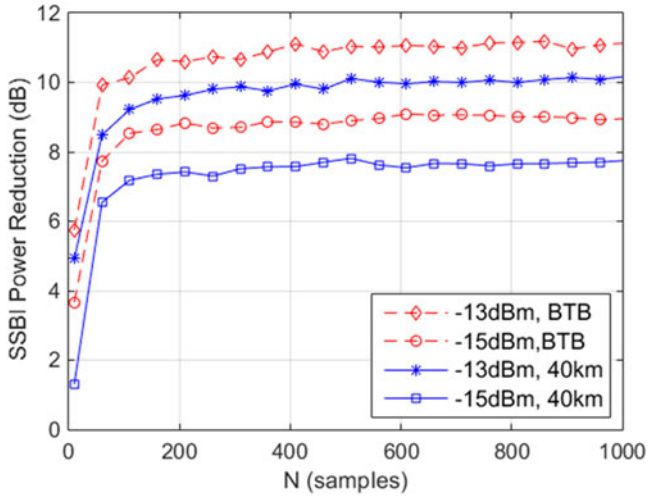

Fig. 9. The average SSBI power reduction as a function of N.

deterioration after 40 km SSMF transmission. Here, the channel responses of the DMT branch are also measured for the two transmission scenarios (see the inset in Fig. 7). In the BTB case, the 3 dB end-to-end channel bandwidth of DMT is about 6 GHz, which is mainly limited by the low-cost electrical amplifier at the transmitter. After 40 km SSMF transmission, its channel bandwidth is reduced to 4.5 GHz and with a sharp roll off from 4.5 to 7 GHz, due to the CD-induced power fading effect. Since the fading period will be more frequent for higher frequency, the transmission capacity of DMT cannot be improved linearly with the increase of bandwidth allocation. But, in contrast to the DMT branch, SSB-OFDM is immune to CD, which exhibits similar BER performance for the BTB and 40 km transmissions. It is demonstrated that the SSB modulation is a better choice for the high frequency components against dispersion distortion than DMT. However, the SSB signal also introduces a mixing SSBI impairment term into the baseband, which has to be compensated after combining the two orthogonal polarization branches together.

We also investigate the performance of the proposed SSBI elimination algorithm. Fig. 8 depicts the digital frequency spectra of $[-7$ GHz, $+7$ GHz$]$ for different SSBI elimination stages. In order to clearly observe the effect of SSBI cancellation, DMT is not modulated on Y polarization here to avoid overlapping with SSBI. Fig. 8(a) shows the spectrum of the actual SSBI product, which is directly extracted from the baseband of $[-7$ GHz, $+7$ GHz$]$ based on the received signal, and (b) shows the spectrum of the estimated SSBI (i.e.,$\hat{A} \cdot |r_{SSB}(k)|^2$, the product of the estimated SSBI

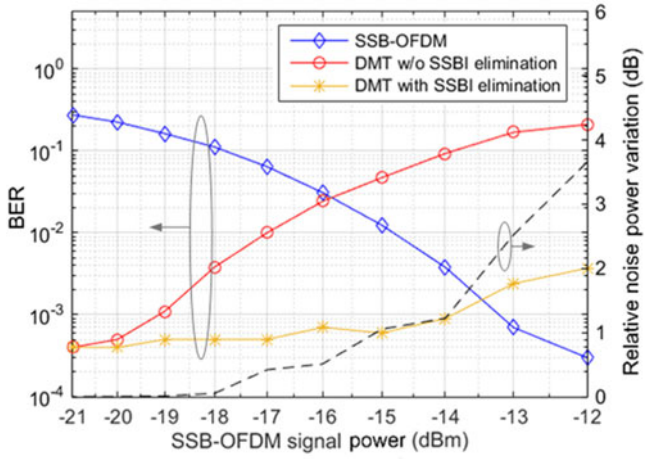

Fig. 10. BER performance comparison (left axis) and relative noise power variation (right axis) as a function of SSB-OFDM signal power.

ratio and the reconstructed SSBI based on the extracted SSB signal). In this case, 200 samples are used to calculate the SSBI ratio $\hat{A}$. After subtracting the estimated SSBI from the extracted term, a flat spectrum can be obtained immediately without any iteration operations, as shown in Fig. 8(c). During the SSBI cancellation processing, the number of samples N used to estimate SSBI ratio is the key parameter. So, we measure the average power reduction of the components in $[-7$ GHz, $+7$ GHz] after SSBI cancellation as a function of N for BTB and 40 km SSMF transmissions at two ROP scenarios. It can be seen that stable performance can be achieved for SSBI cancellation when N is larger than 200 for all the cases. Therefore, N is kept to be 200 for the following processing.

Subsequently, the DMT signal is loaded on Y polarization, and the BER performances are measured with and without SSBI elimination at the different launch powers of SSB-OFDM signal. In this case, the power of DMT is kept at -9 dBm. As a reference, the measured BER performance of SSB-OFDM is also depicted in Fig. 10. It can be seen that the BER performance of DMT can be improved significantly by the use of the proposed SSBI cancellation. Here, the BER of DMT can be kept lower than 1e-3 during the launch power of SSB-OFDM increased from -21 to -14 dBm. However, due to the presence of noise, the estimated SSBI term includes signal-noise beating products. The signal-relative noise would be amplified nonlinearly as the SSB signal power increases (see the black-dashed line in Fig. 10), and which will be imposed on the DMT signal while subtracting SSBI. For this reason, the BER performance of DMT starts to degrade when SSB signal power is larger than -13 dBm. In comparison to the case of SSB signal power at -21 dBm, the increased noise power is in excess of 1 dB for the SSB signal power of -13 dBm. From Fig. 7 and 10, it is interesting to note that there are different power requirements for the SSB-OFDM and DMT signals. In order to achieve the optimum performance, the influence of the power ratio between the two branches are studied. Fig. 11 depicts BER performances of DMT and SSB as a function of the DMT to SSB power ratio-R_{DS} (R_{DS} [dB] $= 10\log_{10}$ (P_{DMT}/P_{SSB}), where P_{DMT} and P_{SSB} are the optical DMT and SSB signal powers respectively) after (a) BTB and (b) 40 km transmissions respectively. Here, the powers of DMT are kept at -2 and 2 dBm for the BTB and 40 km transmissions respectively, and the ROP is kept at -6 dBm for each measured point. It can be seen that the optimum power ratio between the DMT and SSB-OFDM signals is round 5 dB. Because DMT suffers from the CD-induced power fading effect, the optimum power ratio of 40 km transmission is slightly larger ($\sim$0.5 dB) with respect to the BTB scenario. Since the optimum power assignment ratio is known, we employ a 70:30 coupler, instead of using 50:50 coupler, EDFA and tunable attenuators in the following experiments. It can reach a fixed power ratio of 5.5 dB. In this case, the input powers are 13.74 dBm and 9 dBm for IQ modulator and intensity modulator,

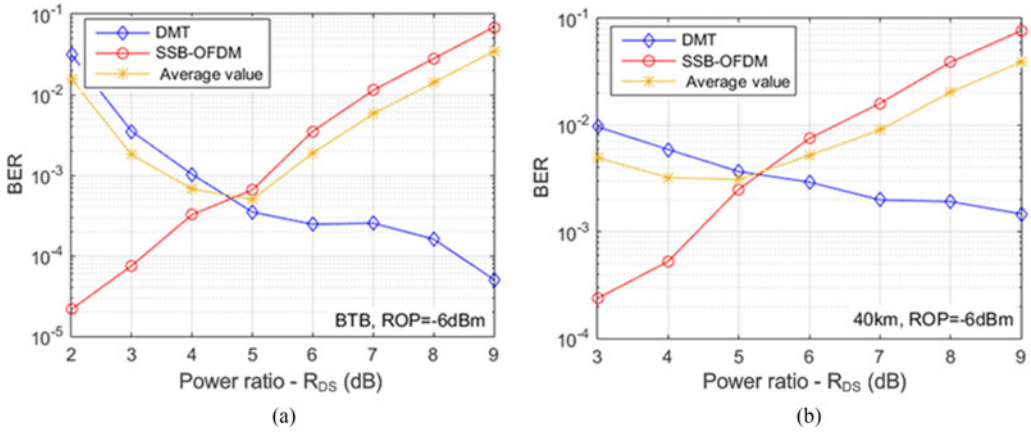

Fig. 11. BER performance as a function of the power ratio between DMT and SSB-OFDM for two scenarios (a) BTB and (b) 40 km transmission (ROP $= -6$ dBm).

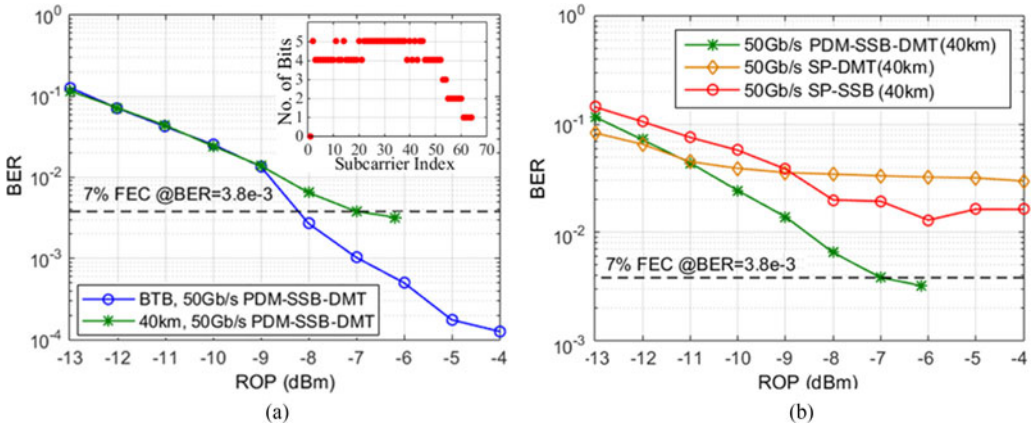

Fig. 12. BER performance as a function of the recovered optical power (a) 50 Gb/s PDM-SSB-DMT with BTB and 40 km SSMF transmissions, (b) different system schemes for 40 km SSMF transmission.

respectively, and the corresponding output powers are -4.5 dBm and 1dBm, respectively. After combining with the PBC, the launch power of PDM-SSB-DMT signal is around 1.8 dBm.

The measured BER as a function of ROP for 50 Gb/s PDM-SSB-DMT signal after BTB and 40 km SSMF transmissions are shown in Fig. 12(a). Here, the maximum ROP is around -6.2 dBm after 40 km SSMF unamplified transmission. The insert of Fig. 12(a) is the corresponding bit loading result for the DMT branch. It can be seen that the receiver sensitivities at BER of 3.8×10^{-3} (with respect to 7% HD-FEC limit) are -8.2 dBm and -7.1 dBm for BTB and 40 km SSMF transmissions, respectively. There is only 1.1 dB ROP penalty after fiber transmission due to the CD-induced impairment. Next, in the same 40 km SSMF transmission scenario, 50 Gb/s PDM-SSB-DMT, SP-DMT, and SP-SSB-OFDM are compared in terms of BER versus ROP as shown in Fig. 12(b). For the fair comparisons of different schemes, the maximum signal bandwidth of 14 GHz is also adopted for the two SP systems. In order to achieve 50 Gb/s transmission data rate, the SP-SSB-OFDM system employs 256-QAM instead of 16-QAM, and SP-DMT system uses the adaptive bit and power loading approach [11] to optimize its performance at the target rate. However, it is apparent that due to the limited SNR for high-order modulation and the CD-induced distortion for IM-DD, the 50 Gb/s SP-SSB and SP-DMT systems both cannot reach a BER of 3.8×10^{-3}. In comparison with these SP systems, the PDM-SSB -DMT system can achieve a good trade-off between the

spectral efficiency and CD tolerance, which in turn enable us to achieve 50 Gb/s PDM-SSB-DMT transmission over 40 km of uncompensated and unamplified SSMF. This will be a cost-efficient solution for the ER (up to 40 km) inter-DC connections.

4. Conclusion

We have experimentally demonstrated a single-end PD based PDM-SSB-DMT system, which can achieve a good trade-off between SE and CD tolerance by the frequency interleave design on two orthogonal polarizations. We detailed the principles of signal modulation, detection and de-multiplexing analytically and also study the key parameters of the proposed system. The optimum launch power ratio is found to be $\sim$5 dB between the DMT and SSB signals. After 40 km SSMF transmission without optical amplification and in-line CD compensation, a 50 Gb/s PDM-SSB-DMT signal can reach the BER of HD-FEC limit at a ROP of -7.1 dBm, which only induce a 1.1 dB penalty relative to the BTB transmission. The PDM-SSB-DMT system will be a promising cost-efficient solution for future extended-reach inter-DC connections.

References

[1] K. P. Zhong *et al.*, "Experimental study of PAM-4, CAP-16, and DMT for 100 Gb/s short reach optical transmission systems," *Opt. Exp.*, vol. 32, no. 2, pp. 1176–1189, Jan. 2015.

[2] W. Kobayashi *et al.*, "25 Gbaud/s 4-PAM (50 Gb/s) modulation and 10-km SMF transmission with 1.3-μm InGaAlAs-based DML," *IET Electron. Lett.*, vol. 50, no. 4, pp. 299–300, Feb. 2014.

[3] C. Yang *et al.*, "IM/DD-based 112-Gb/s/lambda PAM-4 transmission using 18-Gbps DML," *IEEE Photon. J.*, vol. 8, no. 3, Jun. 2016, Art. no. 7903907.

[4] J. Tang, J. He, D. Li, M. Chen, and L. Chen, "64/128-QAM half-cycle subcarrier modulation for short-reach optical communications," *IEEE Photon. Technol. Lett.*, vol. 27, no. 3, pp. 284–287, Feb. 2015.

[5] K. P. Zhong *et al.*, "Experimental demonstration of 608Gbit/s short reach transmission employing half-cycle 16QAM Nyquist-SCM signal and direct detection with 25Gbps EML," *Opt. Exp.*, vol. 24, no. 22, pp. 25057–25067, Oct. 2016.

[6] L. Tao, Y. Ji, J. Liu, A. P. T. Lau, N. Chi, and C. Lu, "Advanced modulation formats for short reach optical communication systems," *IEEE Netw.*, vol. 27, no. 6, pp. 6–13, Nov./Dec. 2013.

[7] M. I. Olmedo *et al.*, "Multiband carrierless amplitude phase modulation for high capacity optical data links," *IEEE J. Lightw. Technol.*, vol. 32, no. 4, pp. 798–804, Feb. 2014.

[8] X. Zhou *et al.*, "Polarization-multiplexed DMT with IM-DD using 2 $\times$ 2 MIMO processing based on SOP estimation and MPBI elimination," *IEEE Photon. J.*, vol. 7, no. 6, Mar. 2015, Art. no. 7802812.

[9] C. Xie *et al.*, "Single-VCSEL 100-Gb/s short-reach system using discrete multi-tone modulation and direct detection," in *Proc. Opt. Fiber Commun. Conf.*, San Francisco, CA, USA, 2015, Paper Tu2H.2.

[10] P. Chow *et al.*, "A practical discrete multitone transceiver loading algorithm for data transmission over spectrally shaped channels," *Trans. Commun.*, vol. 43, nos. 2/3/4, pp. 773–775, Apr. 1995.

[11] R. F. H. Fischer and J. B. Huber, "A new loading algorithm for discrete multitone transmission," in *Proc. Global Telecommun. Conf.*, London, U.K., 1996, pp. 724–728.

[12] H. Bulow, B. Fred, and K. Axel, "Electronic dispersion compensation," *IEEE J. Lightw. Technol.*, vol. 26, no. 1, pp. 158–167, Feb. 2008.

[13] M. Sowailem *et al.*, "Impact of chromatic dispersion compensation in single carrier two-dimensional Stokes vector direct detection system," *IEEE Photon. J.*, vol. 9, no. 4, Jul. 2017, Art. no. 7203110.

[14] Z. Li *et al.*, "SSBI mitigation and the Kramers–Kronig scheme in single-sideband direct-detection transmission with receiver-based electronic dispersion compensation," *IEEE J. Lightw. Technol.*, vol. 35, no. 10, pp. 1887–1893, May 2017.

[15] D. J. F. Barros and J. M. Kahn, "Comparison of orthogonal frequency-division multiplexing and on-off keying in amplified direct-detection single-mode fiber systems," *IEEE J. Lightw. Technol.*, vol. 28, no. 12, pp. 1811–1820, Dec. 2010.

[16] I. B. Djordjevic and B. Vasic, "Orthogonal frequency division multiplexing for high-speed optical transmission," *Opt. Exp.*, vol. 14, no. 9, pp. 3767–3775, May 2006.

[17] A. J. Lowery, L. Du, and J. Armstrong, "Orthogonal frequency division multiplexing for adaptive dispersion compensation in long haul WDM systems," in *Proc. Opt. Fiber Commun. Conf.*, Anaheim, CA, USA, 2006, Paper PDP 39.

[18] N. Liu, C. Ju, and X. Chen, "Nonlinear ISI cancellation in VSSB Nyquist SCM system with symbol pre- distortion," *Opt. Commun.*, vol. 338, pp. 492–495, Mar. 2015.

[19] C. Sanchez, B. Ortega, and J. Capmany, "System performance enhancement with pre-distorted OOFDM signal waveforms in IM/DD systems," *Opt. Exp.*, vol. 22, no. 6, pp. 7269–7283, Mar. 2014.

[20] W. R. Peng *et al.*, "Spectrally efficient direct detected OFDM transmission employing an iterative estimation and cancellation technique," *Opt. Exp.*, vol. 17, no. 11, pp. 9099–9111, May 2009.

[21] Z. Li *et al.*, "Signal-signal beat interference cancellation in spectrally-efficient WDM direct-detection Nyquist pulse-shaped 16-QAM subcarrier modulation," *Opt. Exp.*, vol. 23, no. 18, pp. 23694–23709, Sep. 2015.

[22] J. Huo *et al.*, "50-Gb/s PDM-DMT-SSB transmission over 40 km SSMF using a single photodetector in C-band," in *Proc. Opt. Fiber Commun. Conf.*, Los Angeles, CA, USA, 2017, Paper Tu3D.3.